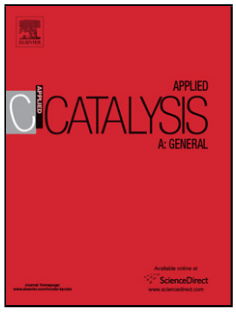

Title: Novel rhodium on carbon catalysts for the oxidation of benzyl alcohol to benzaldehyde: A study of the modification of metal/support interactions by acid pre-treatments

Authors: Conor A. Wilde, Yulia Ryabenkova, Ian M. Firth, Liam Pratt, James Railton, Mariela Bravo-Sanchez, Naoko Sano, Peter J. Cumpson, Phil D. Coates, Xi Liu, Marco Conte

PII: S0926-860X(18)30553-2
DOI: https://doi.org/10.1016/j.apcata.2018.11.006
Reference: APCATA 16875

To appear in: *Applied Catalysis A: General*

Received date: 5 September 2018
Revised date: 29 October 2018
Accepted date: 8 November 2018

Please cite this article as: Wilde CA, Ryabenkova Y, Firth IM, Pratt L, Railton J, Bravo-Sanchez M, Sano N, Cumpson PJ, Coates PD, Liu X, Conte M, Novel rhodium on carbon catalysts for the oxidation of benzyl alcohol to benzaldehyde: A study of the modification of metal/support interactions by acid pre-treatments, *Applied Catalysis A, General* (2018), https://doi.org/10.1016/j.apcata.2018.11.006

Novel rhodium on carbon catalysts for the oxidation of benzyl alcohol to benzaldehyde: a study of the modification of metal/support interactions by acid pre-treatments

Conor A. Wilde,[a] Yulia Ryabenkova,[b] Ian M. Firth,[a] Liam Pratt,[a] James Railton,[a] Mariela Bravo-Sanchez,[c] Naoko Sano,[c,d] Peter J. Cumpson,[c] Phil D. Coates,[b] Xi Liu,[e] and Marco Conte [a*]

[a]Department of Chemistry, University of Sheffield, Sheffield, S3 7HF, UK

[b]School of Engineering, Polymer IRC, University of Bradford, Bradford, BD7 1DP, UK

[c]NEXUS, School of Mechanical & Systems Engineering, Newcastle University, Newcastle upon Tyne, NE1 7RU, UK

[d]Nara Women's University, Nisi-machi, Kita Uoya, Nara, 630-8506, Japan

[e]Syncat@Beijing, Synfuels China Co. Ltd., Huairou, Beijing, 101407, P. R. China

[*]corresponding author E-mail: m.conte@sheffield.ac.uk

Graphical abstract

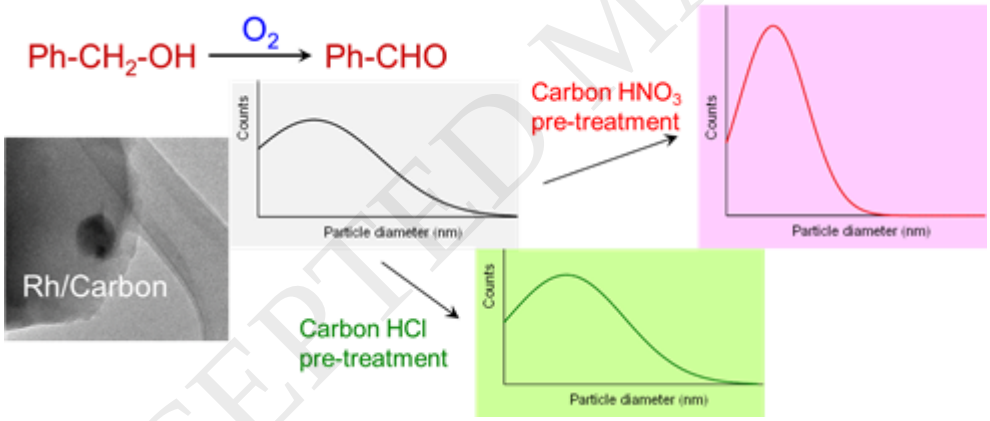

Highlights

• Study of the properties of novel Rh on carbon catalysts for alcohol oxidation under very mild conditions and exploitation of this metal for oxidation reactions.

• A pre-treatment of the carbon support with HNO_3 was reducing Rh particle size, whereas a pre-treatment with HCl was either increasing particle size or had no effect.

• Carbon supports pre-treated with HNO_3 led to enhanced catalytic activity.

- An upper diameter limit for the activity of Rh nanoparticles for benzyl alcohol oxidation was estimated to be ca. 30 nm.

Abstract

Rhodium nanoparticles or rhodium organometallic complexes are mainly used in catalysis for reduction or hydroformylation reactions. In this work instead, we explored the capabilities of Rh nanoparticles as an oxidation catalyst, applied to the oxidation of benzyl alcohol to benzaldehyde under very mild conditions (100 ^{o}C, and atmospheric pressure) as a model reaction. Here we report the preparation of novel Rh/C catalysts by using an impregnation protocol, with particular emphasis on the pre-treatment of the carbon supports by using HNO_3 and HCl, as well as the characterization of these materials by using an array of methods involving TEM, XPS and XRPD. Our preparation method led to a wide Rh particle size distribution ranging from 20 to 100 nm, and we estimate an upper limit diameter of Rh nanoparticles for their activity towards benzyl alcohol oxidation to be ca. 30 nm. Furthermore, a HNO_3 pre-treatment of the activated carbon support was able to induce a smaller and narrower particle size distribution of Rh nanoparticles, whereas a HCl pre-treatment had no effect or sintered the Rh nanoparticles. We rationalise these results by HNO_3 as an acid able to create new nucleation sites for Rh on the carbon surface, with the final effect of smaller nanoparticles, whereas for HCl the effect of sintering was most likely due to site blocking of the nucleation sites over the carbon surface. The roles of acid centres on the carbon surfaces for the oxidation reaction was also investigated, and the larger their amounts the larger the amounts of by-products. However, by treatment with HNO_3 we were able to convert neutral or basic carbons into supports capable to enhance the catalytic activity of Rh, and yet minimised detrimental effects on the selectivity of the oxidation to benzaldehyde.

Keywords: Rhodium, nanoparticles, activated carbons, acid pre-treatment, alcohol oxidation.

Introduction

Rhodium is primarily used in catalysis for reduction or hydroformylation reactions [1, 2]. Very important applications of this metal include the reduction of NO_x to N_2 and O_2 in catalytic converters [3], or the synthesis of acetic acid from methanol, CO and H_2 [4]. In a recent study though [5] we demonstrated that polymer incarcerated Rh nanoparticles can be an efficient oxidation catalyst for the oxidation of aryl alcohols. In particular, a strong catalytic activity was observed in the presence of a biphasic system containing water, in which case Rh can be an oxidation catalyst competitive to more common catalytic systems comprising metals like Au, Pd and Pt [6]. This background prompted us to further investigate the potential of Rh as an oxidation catalyst for alcohol, and especially considering catalysts capable to oxidise alcohols in the absence of a base and without the use of pressurised systems [7]. Furthermore we were also interested to investigate the properties of Rh based catalysts by preparing Rh based nanoparticles supported on activated carbon, using an impregnation protocol [8]. This is a frequent choice in catalysis with a large number of applications ranging from alcohol oxidation [9] to hydrocarbon oxidation [10], as well as halogenation [11] and coupling reactions [12]. The choice of this preparation method is often justified by being a relatively facile preparation protocol and its apparent statistical robustness [13]; whereas the choice of activated carbon as supports is often justified by their high surface area, which together with their structural features - like the presence of phenolic or acid groups - can either reduce an impregnated metal to metal nanoparticles or stabilise high oxidation states at the same time [14]. In addition, surface properties of activated carbon may be altered by treatment with acids [15, 16], and we deliberately used this approach to change the particle size distribution of Rh nanoparticles with the aim to gain structure-activity correlations.

In this context, we were interested to explore the capability of Rh at a fundamental level as an oxidation catalyst - that is by reverting its catalytic activity from a reducing catalyst [17, 18] to an oxidizing species - by using activated carbon of different characteristics as supports for the oxidation of benzyl alcohol to benzaldehyde in the presence of toluene as a solvent. The selection of this reaction as a model system for our study is twofold: alcohol oxidation is one of the most relevant oxidation reactions for the manufacture of fine chemicals [19, 20], and for this class of reactions the oxidation of benzyl alcohol is among the most investigated and understood [21, 22]. As such, this is an excellent benchmark for the investigation of the capabilities of novel materials like those presented and discussed in this study.

In fact, we aim to identify structure-activity correlations for Rh to be used in catalysis as an oxidation catalyst, and to identify particle size ranges and metal support interactions that will

be useful for catalyst development. To the best of our knowledge no information is present in the literature up to which particle size limit Rh may be active as an oxidation catalyst, and little is known [23] about the interactions that Rh centres may have with widely used activated carbons as supports, or the effects that these interactions may have in the oxidation process.

In view of these considerations, we foresee that this work may have broader applications than those focused in this study, by expanding the uses of this metal to novel applications for oxidation reactions and in turn developing the toolkit of nanoparticles available for the synthesis of fine chemicals.

1. Experimental

2.1 Catalyst preparation

All the carbon-supported rhodium catalysts (Rh/C, 1 wt% of Rh content) were prepared using an incipient wetness impregnation protocol [24], using water as a solvent for the dissolution and impregnation of a $RhCl_3 \cdot xH_2O$ precursor (Sigma Aldrich, assay 38 wt%) into the carbon matrices.

Three different kinds of activated carbon were used in this study: Darco-12, Norit GAC 1240 and Norit SA2 (all supplied by Sigma Aldrich and used without any further purification unless otherwise specified). For each of these carbons the macroscopic impregnation volume was preliminary determined by means of calibration curves reporting volume of absorbed water needed to fill the carbon pores against the mass of carbon. These volumes were: 0.90 mL g^{-1}, 0.89 mL g^{-1} and 0.82 mL g^{-1} for Darco-12, Norit GAC 1240 and Norit SA2 respectively. Solutions made of these volumes containing 53 mg of metal precursor were added dropwise with stirring at room temperature to the activated carbons (1.98 g) in order to obtain 2 g batches of catalysts with a final metal loading of 1 wt.%. Each of these products were then dried in static air at 150 ^{o}C (temperature ramp 20 ^{o}C min^{-1}) for 16 h, and used as a catalyst. Control samples in the absence of Rh but comprising acid pre-treated carbons were prepared in an identical manner to the impregnated samples, but without initially adding the $RhCl_3 \cdot xH_2O$ precursor.

The acid pre-treatment of the carbon supports was carried out preparing batches of 5 g of carbon, which were impregnated with HNO_3 (Fisher 68%, 15 M), or HCl (Fisher 32%, 12M), by using incipient wetness impregnation volumes determined as described above. For carbons pre-treated with HNO_3, the stirring was continued at ambient temperature until NO_x

production subsided, for approximately 20-30 min. Each carbon was dried in static air at 150 ^{o}C (temperature ramp 20 ^{o}C min^{-1}) for 16 h [24, 25]. On these pre-treated carbons, incipient wetness impregnation of Rh was carried out. In view of the catalyst preparation procedure used, no filtration of the carbon or catalyst washing was carried out, unless otherwise specified, and the metal loading should be considered as equal to the nominal amount of metal impregnated into the support [26].

Using this procedure, nine different Rh/C catalysts were obtained, (three per each activated carbon), and with each activated carbon comprising: a non pre-treated sample, a sample pre-treated with HNO_3 and a sample pre-treated with HCl). Nine different activated supports were prepared in the same manner but without the addition of Rh, and used for control tests. In this work we use the notation: raw activated carbon (RAC), for supports that have not been treated with any acid, and denoting Darco-12, Norit GAC 1240 and Norit SA2 as RAC1, RAC2 and RAC3 respectively. Activated carbons pre-treated with HNO_3 or HCl are denoted as NAC1, NAC2, NAC3 and HAC1, HAC2, HAC3 respectively. All rhodium containing catalysts use this same notation, preceded by the prefix Rh/ to denote the presence of this metal. For example, a Rh containing catalyst prepared using an activated carbon Darco-12 pre-treated with HNO_3 is: Rh/NAC1.

1.2 Catalyst characterization

1.2.1 Transmission electron microscopy

Samples were prepared for transmission electron microscopy (TEM) analysis by dispersing and sonicating the catalyst powders in high purity ethanol for ca. 10 min, and allowing a drop of the suspension to dry on a lacey-carbon film supported on a 300-mesh Cu TEM grid. Bright-field (BF) images were acquired using a Tecnai G20 TEM microscope operating at 200 keV and equipped with a LaB_6 electron gun. The frequency count for the particle size distribution was obtained from a set of 200 particles for each catalyst. Data analysis and fitting of the particles size distributions by Gaussian and log-normal models was carried out by using OriginPro 2017 software.

1.2.2 X-ray photoelectron spectroscopy

X-ray photoelectron spectroscopy (XPS) was performed with a Kratos Axis Nova spectrometer using a monochromatised AlK_α X-ray source (225 W) with an analyser pass energy of 160 eV for survey scans and 20 eV for high resolution scans. Three positions per

sample were analysed using charge neutralization. All XPS spectra were charge corrected by setting the C1s C-C/H component to 284.8 eV [14].

1.2.3 X-ray powder diffraction

X-ray powder diffraction (XRPD) patterns were acquired using a Bruker D8 Advance equipped with a LynxEye detector. The samples were sieved and deposited over an amorphous silicon sample holder. The instrument was operating at 40 kV and 40 mA selecting the CuKα radiation as X-ray source. The samples were analysed in the range 10^o to 80^o 2θ for a scan time of 71 min.

1.2.4 Acid-base properties of the carbons

Each carbon support RAC1, RAC2 and RAC3 (100 mg) was crushed with a mortar and pestle, dispersed in deionised water (10 mL) and stirred at 700 rpm for 10 min. pH values of the resultant solutions [27] were recorded upon stabilization using an Accumet AB150 pH-meter equipped with a FB67978 ion selective electrode.

1.2.5 Inductive coupled plasma – mass spectrometry

Determination of Fe and Cu content in untreated carbon supports was carried out via ICP-MS analysis. Each untreated carbon, RAC1, RAC2 and RAC3, (1 g) was dispersed in HCl (12 M, 10 mL) under stirring (48 h, room temperature). The resulting suspension was then filtered, and known aliquots of the filtrated solution were analysed using an Agilent 7500CE ICP-MS instrument which was calibrated up to 10 parts per billion (ppb) using standards prepared by dilution from stock solutions containing 1000 parts per million (ppm) of Fe or Cu standards. The concentrations of Fe and Cu in the samples were calculated against a calibration graph.

1.2.6 Inductive coupled plasma – optical emission spectroscopy

A full scan analysis for elemental composition (but C, H and O), was carried out on aqueous extracts from activated carbons by using ICP-OES. Each untreated carbon, RAC1, RAC2 and RAC3, (1 g) was dispersed in HCl (1 M, 5 mL) under stirring (24 h, room temperature). The resulting suspension was then filtered, and the reaming carbon solid was washed 20 times with 5 mL aliquots of deionised water. The resulting liquid filtrate was analysed using a Spectro-Ciros-Vision ICP-OES instrument, which is calibrated for 70 elements. These were are measured on at least two emission lines so any interelement interferences can be avoided.

The plasma conditions were: power 1400 W, coolant flow 12.0 $L \cdot min^{-1}$, auxiliary flow 1.0 $L \cdot min^{-1}$, and nebuliser flow 0.85 $L \cdot min^{-1}$.

1.3 Catalytic tests

The catalyst (200 mg, Rh 1 wt%), was dispersed in toluene (Fluka, 2 mL) and benzyl alcohol (Sigma-Aldrich, 210 mg, 1.94 mmol) solution, in order to obtain a molar metal (Rh) to substrate (benzyl alcohol) ratio, M:S, of 1:100 for each catalyst. For the tests using activated carbon only, a mass of carbon equal to that present in the Rh/C catalysts minus the amount of Rh was used. The reaction mixture was heated using a reflux condenser at 100 ^{o}C for 24 hours with a magnetic stirrer operating at 700 rpm at atmospheric pressure in air.

2.4 Characterization of the reaction mixtures

2.4.1 Nuclear magnetic resonance

Analysis of the reaction mixture to determine product selectivity and conversion was obtained *via* ^{1}H NMR spectroscopy using a Bruker Avance IIIHD 400 spectrometer operating at 400 MHz. NMR spectra were collected using $CDCl_3$ as solvent. Chemical shifts were reported in parts per million (ppm) from tetramethylsilane using the methyl group of toluene resonance as the internal standard (toluene CH_3, s, δ: 2.36 ppm) for ^{1}H NMR [28]. All conversions and selectivity values are expressed in mol %, and all conversion values are based on NMR data (see Appendix A, Supplementary Data File, section S3), on the observed products. In fact, GC/MS characterizations (*vide infra*), revealed only traces amounts of by-products < 1% which are due to condensation reactions from isomers of methyl-diphenylmethane. Due to their very low amount these could be neglected in our selectivity calculations by normalizing all the selectivites to the presence of: benzaldehyde, benzyl ether and methyl-diphenylmethane isomers. Functional groups for quantification of species in the reaction mixture and comparison with standard compounds of benzyl alcohol, benzaldehyde, dibenzyl ether, 4-methyl-diphenylmethane and benzoic acid are reported in detail in supplementary data (Figs. S1-S4), as well as a description of the formulas used to calculate conversion and selectivity (eqs. S1-S5).

2.4.2. Gas chromatography – mass spectrometry

Gas chromatography mass spectrometry analysis was used for the characterization of the reaction mixtures and analysis of traces. GC/MS was carried out using a Perkin Elmer

Turbomass GC-MS, equipped with a Phenomenex Zebron ZB-5MS column 30 m × 0.25 mm, 0.25 μm film thickness. The carrier gas was helium at 1 mL min^{-1}, the injection volume was 1.0 μL, using an injector temperature of 250 ºC, and a temperature programme from 60 ºC to 260 ºC using a ramp at 10 ºC min^{-1} and then hold for 10 minutes.

2.5. Computational studies

Quantum chemical calculations were performed using Gaussian 09, version D.01, [29] running on a 32 processor (Viglen) 64-bit computational Linux cluster. Mixed basis sets coupled with density functional theory (DFT) methods and the effective core potential were used. In detail, mixed basis sets SDD (Stuttgart-Dresden triple ζ incorporating effective core potentials) for the transition metal Rh [30], and 6-311G(d,p) (Pople triple split valence Gaussian basis functions with added polarization) for all other non-transition-metal atoms have been employed [31], using the B3LYP functional of DFT [32]. The nature of stationary states (minimum structures) was confirmed by frequency calculations. Stabilization energies of the complexes were obtained by subtraction from energetic values of isolated species, and considering zero point energy (ZPE) corrections [33] for all of the molecular structures.

2. Results and discussion

3.1 Catalytic activity of Rh/C catalysts prepared on untreated activated carbon supports

Rhodium supported nanoparticles (Rh 1 wt%) were prepared over activated carbons by using three among the most common activated carbons used in catalysis, namely: Darco-12 [34], Norit GAC 1240 [35] and Norit SA2 [36]. These are used for their large surface area, acid/base properties and granulometry and they are here abbreviated for simplicity as RAC1, RAC2 and RAC3 respectively. These carbons were initially used untreated as supports for Rh nanoparticles. The resultant Rh/C catalysts, as well as the carbon supports only as control tests, were tested for the oxidation of benzyl alcohol to benzaldehyde as a model reaction (Table 1), and under very mild conditions (T = 100 ºC, P = atmospheric pressure of air). This, with the aim to determine the catalytic capabilities of Rh species for oxidation reactions, by using a facile impregnation protocol.

All the Rh/RAC catalysts are able to oxidise benzyl alcohol to benzyl aldehyde (Scheme 1(a), and Figs. S5-S7), although to a different extent. The most active catalyst, in terms of

conversion, is Rh/RAC1 (52%) with the trend: Rh/RAC1 > Rh/RAC2 > Rh/RAC3. The selectivity to benzaldehyde follows an opposite trend instead: Rh/RAC1 < Rh/RAC2 < Rh/RAC3, with a selectivity up to 100% for the latter catalyst. In contrast, when Rh/RAC1 is used, products like dibenzyl ether and methyl-diphenylmethane are detected (Fig. S5). Whereas the presence of dibenzyl ether may be related to condensation of two molecules of benzyl alcohol with de-hydration (Scheme 1(b)) [37], the presence of methyl-diphenylmethane as a by-product (Scheme 1(c)) is rather surprising, as this compound is usually obtained via benzylation of toluene with benzyl alcohol over strongly acidic zeolites [38], and not by using activated carbons. Nevertheless, the presence of this by-product was confirmed via GC-MS and comparison with standards (Figs. S8 and S9), with the identification of two isomers (2- and 4-methyl-diphenylmethane).

These four compounds: benzyl alcohol, benzaldehyde, dibenzyl ether and methyl-diphenylmethane are also the major components of all of our reaction mixtures with a carbon mass balance > 95% in all cases. This was obtained by calibration of the signal of toluene used as internal standard (see supplementary data, eqs. S6-S11), thus confirming these are the only products of our reaction.

In this context, it does worth to highlight that we did not detect any formation of benzoic acid in reaction mixtures using catalysts prepared using the untreated supports, nor in reaction mixtures from catalytic tests using the catalysts prepared via acid pre-treatment. As benzoic acid is obtained from benzaldehyde via a free-radical pathway involving the formation of acyl radicals which evolve to peracids [39], and in turn decompose to acids, we speculate that the carbon supports may quench acyl radicals, thus inhibiting this reaction pathway.

Furthermore, in order to explain the product distribution described in scheme 1, it should be noted that although activated carbons are not as acidic as zeolites, they may still be acidic or have different acid-base properties. In particular, we confirmed [27] RAC1 is an acidic carbon (pH water extract = 4.7), whereas RAC2 and RAC3 are basic carbons (pH water extract = 9.9, and 10.5 respectively). This suggests that the presence of dibenzyl ether when Rh/RAC1 and Rh/RAC2 are used, is a consequence of the acid-base properties of the activated carbon supports rather than an effect induced by Rh nanoparticles. As confirmed by control tests by using the activated carbons only in the absence of any Rh (Table 1 bottom). In fact, Rh/RAC1 and RAC1 as well as Rh/RAC2 and RAC2 both led to dehydration

products, whereas Rh/RAC3 and RAC3, the most basic of the carbons, led to the formation of benzaldehyde only.

To further corroborate this experimental evidence, and support our hypothesis for the formation of dibenzyl ether and methyl-diphenylmethane methyl-diphenylmethane isomers, we added acids: HCl, HNO_3 and H_2SO_4 into an alcohol/toluene mixture (Table S1). The principle of these tests was the following: HCl to act as an acid catalyst only, HNO_3 as an acid but capable of oxidation processes, and H_2SO_4 as an acid with strong dehydration capabilities. HCl led to a small conversion (< 10%) and a mixture of dibenzyl ether and benzyl methyl benzene, HNO_3 led to a conversion of ca. 10% and benzaldehyde only as product. H_2SO_4 led to a conversion > 90% and was selective to methyl-diphenylmethane (Table S1). This trend broadly fits the properties of these acids. In view of these tests, we conclude that Brønsted acid sites on RAC1, and in minor part on RAC2, are those responsible for the observed by-products and product distribution. It does worth noting though, that even if HNO_3 is capable to carry out the oxidation of benzyl alcohol to benzaldehyde, it cannot be practically used as a reagent as it would eventually corrode the walls of a catalytic (non-glass) reactor.

Furthermore as the formation of methyl-diphenylmethane via benzylation is also a consequence of a dehydration reaction but with toluene as a reagent, and not just as a mere solvent (Scheme S2), we tested the Rh/RAC catalysts and solvent-free benzyl alcohol as a substrate (in this case by using a M:S ratio of 1:1000, Tables S2-S4) No methyl-diphenylmethane was detected, thus confirming this by-product is a consequence of a reaction between the solvent and the substrate and the acid properties of the carbon support (RAC1).

The solvent-free tests are important also for an additional reason. Alcohols may disproportionate to lead to the formation a carbonyl containing compound and an alkane [40]. In our case this reaction would be: $Ph\text{-}CH_2\text{-}OH + Ph\text{-}CH_2\text{-}OH \rightarrow Ph\text{-}CHO + Ph\text{-}CH_3 + H_2O$. However, we did not detect any formation of toluene during our tests, most probably as this reaction is promoted in basic media [41] or biphasic systems [5].

In summary, the catalytic activity of Rh/C catalysts (Table 1) should be considered as the result of two distinct contributions: (a) a contribution form Rh species oxidising benzyl alcohol to benzaldehyde, and (b) a contribution from the activated carbon supports (mainly

RAC1) responsible for the formation of by-products: benzyl ether and methyl-diphenylmethane.

On the other hand, the activated carbons alone, especially RAC1, were also capable of some catalytic activity towards the formation of benzaldehyde in the absence of Rh. In contrast the activity of RAC3 is the same, within experimental error, to the background activity of the blank reaction (ca 5%). To explain these carbon behaviours, and verify the origin of this minor oxidation process, we carried out additional control tests. Activated carbons are known to contain Cu of Fe, which can oxidise an alcohol via reaction pathways involving peroxides in solution [42-44]. As a consequence, we quantified the amounts of these metals in our carbons via extraction and ICP-MS methods. The metal content for Cu and Fe was ranging from 0.01 to 0.1 wt% (Table S5). In order to rule out possible interference to the catalytic activity from the presence of these metals, the activated carbons were then washed by using diluted HCl (see supplementary data for experimental details) to remove metal contaminants natively present within the carbon [11] .

However, upon testing the activated carbons after these treatments (Table S6) both the conversion and the selectivity were virtually identical (i.e. within our experimental error) to those of un-washed carbons (Table 1). This leads us to conclude that although traces of Cu and Fe are present in our samples, these do not contribute to the activity or our catalysts, and the oxidation activity that we observe from the carbons may originate from reaction pathways involving the formation of peroxides in solution in the absence of metals [45]. Activity which, however, is very close to that of blank tests. As a consequence, we conclude the activated carbons can be used for our reaction without any further purification steps.

Nevertheless, in order to gather data for a more comprehensive comparison on the effect that the different activated carbons can induce to our reaction or to the Rh nanoparticles, we carried out a full elemental scan on aqueous extracts (see experimental section 2.2.6) of the activated carbons and analysed these samples via ICP-OES (Tables S7-S10). Up to 26 elements were identified, with Fe being indeed among the most abundant species, together with Al, Ca and Mg. Unlike RAC2 and RAC3 though, we observed the presence of significant amount of S for RAC1 (2.5 mg of S per gram of activated carbon, accounting for ca. 30 at% of the total impurities). Whereas the presence of S is not uncommon in activate carbon via thiols groups [46] these could act as nucleation centres for Rh. A factor to be considered for future catalysts development, for metals supported nanoparticles not restricted to Rh, but extendable also to metals like Pd or Au which show a greater affinity for S rather than O.

3.2 Expected effects on metal-support interaction by activated carbon pre-treatment with HNO_3

By comparing the data reported in table 1, it is evident that Rh displays some appreciable activity, however we speculated how to increase the conversion of these catalysts but still preserving good selectivity for benzaldehyde. An obvious parameter to be considered in this sense is Rh particle size. In fact, control tests by using $RhCl_3 \cdot xH_2O$ did not show any appreciable catalytic activity, conversion < 5%, and consistent with blank values (Table 1), and therefore not statistically showing any activity. With our preparation method it is the carbon itself to be a reducing agent [24] for Rh^{3+} centres to Rh^0 species, or to a combination of Rh^{3+}/Rh^0 species. On the other hand, in order to trigger the nucleation and formation of nanoparticles, Rh^{3+} species from a precursor in solution need to anchor to the carbon support in the first instance [47]. This circumstance prompted us to consider a pre-treatment of our carbon matrices before the deposition of Rh. This with the aim to: (i) induce a change in Rh particle size distribution, (ii) estimate a Rh particle size upper limit for the activity of this metal for our model reaction, and (iii) gather an estimate on the efficiency of an impregnation protocol in terms of uniformity of final Rh size without any post-reduction treatment. The latter to form the basis of a future work involving the identification of the active sites for this reaction, which at present is beyond the purpose of the current manuscript.

Activated carbons are complex matrices containing phenol, ethers, esters and carboxylic acids on their surfaces [48]. Among these functional groups, carboxylic acids are excellent functionalities for the coordination of metallic cationic species [49]. In view of this, the principle to change particle size distribution, and in turn change or enhance the activity of our catalysts is the following: as HNO_3 is an oxidizing agent, we would oxidise either hydroxyl groups to aldehydes or acids [50], or methyl and methylene groups to acid (eq. 1) and carbonyl (eq. 2) groups respectively [51]:

$$R\text{-}CH_3 + 3HNO_3 \rightarrow RCOOH + 3HNO_2 + H_2O \qquad \text{(eq. 1)}$$

$$R\text{-}CH_2\text{-}R + 2HNO_3 \rightarrow R\text{-}CO\text{-}R + 2HNO_2 + H_2O \qquad \text{(eq. 2)}$$

A pre-treatment of the activated carbon with this acid should then increase the amount of carboxylic acids on the carbon surface, and in turn the amount of nucleation centres available

for the initial coordination of Rh^{3+} species. A similar process has been observed for Cu over activated carbon materials via the general scheme (eq. 3) [51]:

$$X\text{-}OH + M^{n+} \rightarrow X\text{-}O\text{-}M^{(n-1)+} + H^{+} \qquad \text{(eq. 3)}$$

Where X is any organic branch, including carbonyl groups, of the carbon framework, most often a phenol or a carboxylic acid. It should also be noted that any residual HNO_3 in our catalysts is eliminated by virtue of our calcination process in air at 150 ºC, which is used promote the reduction reaction (eq. 4) [25]:

$$4HNO_3 \rightarrow 4NO_2 + 2H_2O + O_2 \qquad \text{(eq.4)}$$

and in turn oxidation of the activated carbon. As the total amount of Rh precursor is a constant across all our tests, a higher amount of nucleation centres should translate to smaller Rh particles over our catalysts, and possibly a higher activity (Scheme 2). For this procedure to be effective though, we would not have to increase the amount of acid centres so much to lead to the formation of undesired by-products by Brønsted acid centres.

In order to further corroborate this working hypothesis, we carried out some DFT studies aimed to mimic the interaction of a $RhCl_3$ precursor with different functional groups on the activated carbon surface. The principle of this approach is the more stable the interaction of $RhCl_3$ with a carbon functional group, the higher the likelihood to act as a nucleation centre, and in turn initiate the nucleation process, or formation of nanoparticles on that group.

To this purpose, we used a simplified, and yet useful, model by evaluating the interactions of $RhCl_3$ with: benzene, *p*-xylene and naphthalene to mimic the interaction of a Rh centre with a carbon basal plane (Figs. S10(A-C)). As well as propane, propanol and propionic acid (Figs. S10(D-F)), *p*-xylene, *p*-toluic alcohol and *p*-toluic acid (Figs. S10(G-I)) to investigate the evolution on adsorption capabilities, and in turn nucleation, of a $-CH_3$ end to a R-OH and R-COOH functional groups.

Although basal planes can have a strong stabilization of the $RhCl_3$ precursor, from just −29 $kJ{\cdot}mol^{-1}$ for a single benzene ring, to −336 $kJ{\cdot}mol^{-1}$ if naphthalene is considered (Table S11), these centres would not allow for the dissociation of Cl^- and in turn initiate the nucleation process.

By considering the series propane, propanol and propionic acid to assess the evolution in adsorption strength from a $–CH_3$ end to a –COOH end. The acid can form a complex with $RhCl_3$ with a stabilization energy of stabilise the $RhCl_3$ precursor of –68 $kJ{\cdot}mol^{-1}$ against a stabilization energy of just –10 $kJ{\cdot}mol^{-1}$ for an alkyl $–CH_3$ end. Thus showing the appropriateness of our approach and the need to functionalise the activated carbon (Table S11). From our simplified model it would also appear an alcoholic function could stabilise a $RhCl_3$ precursor more than the acid, with a stabilization energy of –106 $kJ{\cdot}mol^{-1}$. It does worth nothing though, that in all our complexes, the H atom of the COOH group is facing in the opposite direction with respect to the $RhCl_3$ complex. In fact, if complexes were built with the H atom of the COOH facing the $RhCl_3$ complex, unstable species comprising imaginary frequencies were obtained, and implying the attack of a Cl ligand by H to form HCl, and dissociate the complex. This same trend was observed if *p*-toluic acid was used for our models, and similar stabilization energies (Table S11) were also observed. This phenomenon on the other hand, is precisely the start of the nucleation process. At present stage, and with our simplified model, we can corroborate our hypothesis that acid functional groups are indeed nucleation centres for Rh nanoparticles. It follows that an oxidation of the carbon support would lead indeed to a larger amount of nucleation sites, either these be al alcohol or an acid, and ultimately smaller nanoparticles.

3.3 Catalytic activity of Rh/C catalysts with supports pre-treated with HNO_3

The effect of a HNO_3 pre-treatment of the activated carbon to the catalytic activity, was systematically evaluated for both: Rh/AC catalysts and activated carbons only as control tests (Table 2).

It is possible to observe (Table 2 and Figs. S11-S13) that a HNO_3 pre-treatment was capable to increase the activity of all untreated Rh/RACs carbons systematically, with relative conversion enhancements ranging from +40% for Rh/NAC1 to nearly +90% for Rh/NAC3, if compared to Rh/RAC1 and Rh/RAC3 (Table 1). However, this also led also to an increase in by-products (especially MDM) for Rh/NAC1 and Rh/NAC2. In contrast, the conversion of Rh/NAC3 was nearly doubled, to a significant 37%, but still preserving a 100% selectivity to benzaldehyde. As such, we consider this kind of pre-treatment a powerful tool to modify, and possibly enhance, the catalytic activity of Rh species, which could potentially find a wider applicability to other metals or supports. We ascribed this enhancement in catalytic activity to a narrower particle size distribution and smaller Rh particle size as compared to the original Rh/RACs catalysts (see section 3.4).

Furthermore, in analogy to the tests and data showed in section 3.1, the pre-treated carbons without any deposited rhodium were also tested (Table 2 bottom). It is evident that the HNO_3 treatment increases the background activity of the activated carbon matrices too, with the formation of non-negligible amounts on dibenzyl ether and methyl-diphenylmethane for NAC1 and NAC2. On the other hand, as we previously demonstrated (see section 3.1) these by-products originate from Brønsted acidity from the activated carbons, these data also indirectly prove that by using HNO_3 we are indeed converting carbon functional groups to carboxylic functional groups.

3.4 Catalytic activity of Rh/C catalysts with supports pre-treated with HCl

In view of the effects induced by HNO_3, we pre-treated the activated carbons with HCl before the deposition with Rh. As HCl does not have any oxidising nature, this acid should not affect the activity of the carbon matrices, i.e. without inducing any changes in carbon functional groups. On the other hand, the presence of Cl^- ions could still affect the final Rh particle size, in this case Rh should behave like Au or Pt, as for these metals experimental evidence shows a sintering effect of Cl^- ions towards the formation of Au and Pt nanoparticles **[52].** In analogy to the experimental approach used in sections 3.1 and 3.2, Rh was impregnated into activated carbon matrices pre-treated with HCl, and pre-treated activated carbons in the absence of Rh were also tested as control test (Table 3).

Interestingly the activity of these catalysts, both in terms of conversion or selectivity, is the same or lower than the untreated catalysts (Table 1 and Figs. S14-S16). Thus proving HCl does not significantly affect the surface of the activated carbons, but it may increase the Rh particle size or have a small poisoning effect. Regarding the effect on the particle size of impregnated metals, studies on the adsorption or binding of Cu centres on carbon surfaces [51] showed that HCl may hinder the availability of nucleation sites (eq. 6) and especially if Cl^- ions are present in large excess.

$$XOH + HCl \rightarrow XCl + H_2O \qquad \text{(eq. 6)}$$

In this hypothesis Cl^- ions that would coordinate on the surface of the carbon in place of the metals. If this model is correct, and by virtue of our approach (Scheme 2) in our case the metal nanoparticles may be bigger not because the Cl^- ions are directly affecting the sintering of metallic species, but because diminishing the number of functional groups available as nucleation centres, and only in turn an increase in the particle size. Incidentally, this effect

could be operating also for Au and Pt and explain the sintering effect of Cl^- for these metals in a different perspective [52].

3.5 Characterization of the catalysts and structure-activity correlations

In order to identify and confirm structure-activity correlations to our product distribution, both with respect to Rh particles size and changes in activated carbon structure (especially changes of functional groups), the catalysts were characterised by using TEM, XPS and XRPD.

3.5.1 Transmission electron microscopy, Rh particle size and distribution

Changes in particle size are crucial in many catalytic applications [53] and the principle of the use of HNO_3 was precisely to induce these changes. In order to experimentally verify this hypothesis, particle size and distribution of Rh nanoparticles were evaluated systematically via TEM for all of the nine Rh/ACs catalysts.

It should also be underlined that TEM analysis of these samples is not trivial due to the extreme dispersion of the active metal component, which presents a 1 wt% metal loading over materials with surface areas of ca. 600 $m^2 \cdot g^{-1}$ [54], 1060 $m^2 \cdot g^{-1}$ [55] and 660 [56] $m^2 \cdot g^{-1}$ for RAC1 (Darco-12), RAC2 (Norit GAC 1240) and RAC3 (Norit SA2) respectively. Nevertheless, we were able to collect images comprising sets of 200 particles per catalyst and therefore appropriate for statistical purposes and a meaningful data analysis of our results [57]. Representative TEM images for each catalyst, together with their particle size distribution are shown in Fig. 1(A-I).

TEM analysis of these samples lead to a number of interesting features: (i) a very large average particle size range (mostly from 20 to 100 nm, with a small population of particles even in the range of 200 nm), (ii) the lack of uniform size distributions, and with large standard deviations from 10 to 50 nm, and (iii) only a few distributions appear to have a Gaussian profile (for example Rh/NAC1, Rh/RAC3 and Rh/HAC3), whereas most of the others appear to be highly skewed. It is worth to consider that impregnation protocols are known to induce both large particle sizes and non-uniform distributions [58]. Nevertheless, when applied to Rh, this method appears to lead to a much larger distribution and non-uniform particles if compared to metals like Au or Pd. For these metals particle sizes in the range of 2 to 20 nm can be obtained [11,15], and by using similar activated carbons as well as

low metal loading like those we have used. This experimental evidence may be due to intrinsic properties of Rh when this protocol is applied to this metal. Surface energy calculations by embedded atom methods [59] show that Rh has a higher surface energy compared to Au and Pd. If these models are correct, Rh may minimize this energy by leading to nanoparticles with a lower surface-to-bulk ratio i.e. larger nanoparticles. It should be noted though that it is possible to synthesise Rh nanoparticles as small as 3 nm, but by using incarceration methods [5].

Furthermore, in order to account for the skewing of the particle size distributions, these distributions were fitted by using a standard Gaussian model [60] (eq. S12 and Fig. S17(A-I)), and a log-normal distribution model [61] (eq. S13 and Fig. S18(A-I)). The latter distribution is not uncommon to fit nanoparticles [62], although it is more often found in nanoparticle distributions obtained from colloids or embedded into polymeric matrices [63]. A summary of these fittings is reported in table 4.

Although for the catalysts Rh/RAC1, Rh/NAC1, Rh/NAC2 and Rh/HAC1 the differences between these two fitting models is small and their averages are similar (and effectively statistically identical given the large dispersion of our data), the catalysts: Rh/RAC3, Rh/NAC1, and Rh/HAC3 are better described by a Gaussian distribution, whereas the marked skewed particle size distribution for Rh/RAC2, Rh/NAC3 and Rh/HAC2 is better described by a log-normal distribution.

By using this data treatment and by selecting the best fitting model for each catalyst, we can estimate the Rh/RAC catalysts have an average particle size of: 30 nm, 29 nm and 69 nm for Rh/RAC1, Rh/RAC2 and Rh/RAC3 respectively. With the catalyst with the largest particles being also the least active (Table 1).

In contrast, when the carbon support is pre-treated with HNO_3 a smaller average particle size, and in general also a narrower distribution, is obtained with diameters of: 23 nm, 31 nm and 32 nm for Rh/NAC1, Rh/NAC2 and Rh/NAC3 respectively. And as such corroborating our hypothesis of a smaller particle size by a HNO_3 pre-treatment, and in turn catalysts inherently more active for the oxidation reaction.

For the effect of HCl towards the formation of Rh nanoparticles, this appears more difficult to predict or interpret. Diameters of 20 nm, 36 nm and 106 nm were obtained for Rh/HAC1, Rh/HAC2 and Rh/HAC3 respectively. However, Rh/HAC1 presents smaller particles than

the untreated sample Rh/RAC1, but a similar range if compared to Rh/RAC2, and a much larger diameter if compared to Rh/RAC3.

Taking these trends as a whole, it appears that a pre-treatment with HNO_3 lead to smaller Rh particles or a narrower particle size distribution compared to samples obtained from untreated carbons. Whereas a pre-treatment of the support by using HCl does not lead to any obvious trend. Given these results though and the different functionalities over our activated carbons, these effects may also be a function of the concentrations and amounts of the acids used to carry out these treatments [64]. A parameter, the evaluation of the concertation effect, which although beyond the proof of concept of the present manuscript, could be considered for future catalyst development.

3.5.2 Rh particle size range and activity

It is obvious that these particle size ranges are very wide, and we think it is unrealistic to consider such large particles (like those from Rh/HAC3 in the range of 100 nm) to be active towards the oxidation reaction. In other terms, a factor or parameter is the *effect that a pre-treatment* has on the Rh particle size, but another factor or parameter is the *effect of changes in Rh particle size* has on the catalytic activity. As a consequence, and in order to provide some estimate beyond which limit these nanoparticles are not active anymore, we grouped all the data in one diagram, and reported also the overall range of activity of the activated carbon supports (Fig. 2). Noteworthy, for particles above *ca.* 30-40 nm no changes or correlations with the catalytic conversion are observed anymore, suggesting the particle size would not be an active parameter anymore.

Therefore, we consider this value as an approximate upper limit diameter for the activity of Rhodium for this oxidation of benzyl alcohol, or conversely to be active for this reaction requires to be smaller than roughly ca. 30 nm. We deem this conclusion, although being a broad estimate, to be relevant for future catalyst development based on this metal.

3.5.3 X-ray photoelectron spectroscopy of Rh/ACs catalysts

XPS is often used to characterize carbon matrices [65] to investigate changes in surface functional groups like the presence of single or double C-C bonds, as well as carbonyl, alcohol or ether groups [66], by analysing C1s and O1s signals, and in the present work XPS has been used precisely for this purpose. On the other hand, one of the major uses of XPS is also to investigate atomic composition and oxidation state of active metal components on the surface of the support [15, 26].

In our case a detailed XPS analysis was carried out for all of our nine catalysts (3 × Rh/RAC, 3 × Rh/NAC, and 3 × Rh/HAC); however, we should note that with respect to the surface atomic composition, no Rh signal was detected. We ascribe this result to an intrinsically low signal for Rh and that our Rh centres are extremely dispersed in our carbon matrix, with in turn a very low exposed metal fraction for a meaningful detection, as also confirmed by XRPD analysis (see section 3.4.5).

As a consequence, we focused our attention to XPS signals originating from the carbon matrices only, and more specifically to the peak fitting of the C1s region. In fact, the samples contain some SiO_2, more specifically quartz, as detected also by XRPD (see paragraph 3.4.5), which is not uncommon for activated carbons [67]. However, due to the relative high intensity of Si2p (103.5 eV) in the XPS surveys, this would imply a significant O1s peaks at ca. 533 eV [68], which fully overlaps with the O1s peaks originating from the carbon matrices themselves ranging from 531 to 535 eV. As a consequence of these factors, and with the aim to produce a meaningful data analysis, O1s has not been included and we focused to the peak fitting of the C1s peak only.

The C1s signals were peak fitted (Fig. 3(A-I)) by using three components at: (i) 284.6 ± 0.2 eV assigned to C-C and C=C bonds [69], (ii) 286 ± 0.2 eV assigned to C-OH and C-O groups [70], and (iii) 288.2 ± 0.2 assigned to C=O and O-C=O groups [71].

By carrying out this data treatment, the composition ratios of the three chemical groups were calculated from the peak fitting (Table 5).

From these data a systematic effect is present: every catalyst obtained by pre-treating the activated carbon with HNO_3 has a greater relative amount of carbonyl groups, if compared to catalysts obtained from untreated carbons. This shows that HNO_3 is indeed oxidising the carbon surface [16, 64]. And this also corroborates our initial hypothesis that if a higher amount of acid (carbonyl) centres is present, then the smaller the particle size and the higher activity, and this also well correlates with our activity trends and TEM data. For the catalyst obtained from carbons pre-treated with HCl no clear trend is observed instead. However, this also indirectly correlates with TEM data, where no clear trend with respect to treatment/activity was observed for these catalysts.

3.5.4 X-ray powder diffraction of Rh/ACs catalysts

XRPD patterns were collected (Fig. 4(A-C)) to further complement TEM and XPS data concerning the status of Rh in our materials (i.e. dispersed nanoparticles), and to identify

possible changes in the carbon structure, for example the presence or modifications of graphitic carbon due to our acid pre-treatments.

Concerning rhodium species, no diffraction peaks for the Rh facets {111}, {002} and {022} (expected at 41.07º, 47.79º and 69.89º 2θ respectively) [72], nor diffraction peaks for the Rh_2O_3 oxide facets {112}, {220} and {312} (expected at 34.49º, 48.80º and 62.07º 2θ respectively) [73] were detected. In general terms, the lack of these diffraction peaks could imply: (i) a particle size of below 4-5 nm, (ii) a thin layered metal structure or (iii) highly dispersed metal species and in turn a very low metal exposed fraction [74, 75]. As TEM revealed very large particles in the range of tens of nm, but XPS did not detect any Rh signal, these methods rule out hypotheses (i) and (ii) and leave case (iii), a very low exposed fraction, as the reason for the lack of detection of Rh signal in our patterns.

However, given the method that we have used to prepare our catalysts (see section 2.1), we postulate our nanoparticles to be a combination of Rh and Rh_2O_3 species. The formation of Rh_2O_3 species would be a consequence of the interaction of Rh with oxygenated groups over the carbon surface responsible for the nucleation process (see sections 3.1 and 3.2), and the formation of Rh centres a consequence of a reduction process induced by the carbon [11, 14, 76]. In this context we also prepared a Rh/RAC3 material comprising up to 10 wt% or Rh (Fig. S19); however, also in this case, no obvious XRD reflections could be detected due to the dispersion of our species into and on the carbon matrix.

Regarding a pattern analysis of the activated carbon supports instead, the only feature that appears evident is the presence of inclusions of quartz in all the samples. Reflections at: 20.85º, 26.65º, 36.54º, 50.14º, and 59.95 º 2θ, for the facets {100}, {101}, {110}, {112} and {211} respectively [77], thus fully matching XPS data and the presence of SiO_2. These inclusions are particularly noticeable in AC1 and AC3 containing materials, with only minor amounts in AC2. This well reflects the origin of these activated carbons: lignite coal for RAC1 (Darco-12) [54], bitumen for RAC2 (Norit GAC 1240) [555], and peat for RAC3 (Norit SA2) [56].

For all these samples though, no clear evidence of any graphitic carbon, for which a characteristic reflection at 25.6º 2θ would be expected for the {002} facet, is detected. Other reflections, although less intense, that would be expected at 24.1º, 25.2º 2θ [78], or in the range of 43º 2θ, and characteristic of reflections associated to graphite basal planes [79]. (i.e.

surface platelets with maximum electron conjugation), are also not detected Moreover, it also appears that whereas there are some small differences among the various activated carbons, there is no detectable difference within the same activated carbon upon acid treatment, either comparing fresh carbon supports or materials comprising Rh. In summary, we can then conclude that any effect induced by the acid pre-treatments involves only the surfaces of the carbon matrices, but not their bulk structure.

3.6 Effect of catalyst grain size of the activated carbons on the catalytic activity

Finally, in order to complete the comparison for the activity of our catalysts, we took into account the different granulometry of our materials as an additional factor that might contribute to the catalytic trends we reported so far. In fact, the activated carbons we have used, have the following average grain size (expressed as sieve diameter) of: 3.8 mm, 1.4 mm and 0.18 mm for RAC1 (Darco-12), RAC2 (Norit GAC 1240) and RAC3 (Norit SA2). The sieve diameter is the minimum width a granule can pass through a sieve of specified mesh if orientated correctly [80]. These diameters, in principle, may sufficiently differ to contribute to our catalytic results by affecting both conversion and selectivity [65] by diffusional limitations.

In view of this, and to carry out a set of comprehensive control tests, all of the catalysts and all the carbon supports, un-treated and pre-treated were ground and sieved by collecting a fraction between 100 and 200 μm. This fraction was selected because for slurry-type reactors [81] (like in our case: a liquid and a gas that react over a solid), and that utilise small catalyst particles, diffusion is considered negligible and this is also a grain size range that is the closest to the smallest activated carbon we have used: RAC3 (Norit SA2).

These control tests (Tables S12-S14) showed that no significant change is detected for the conversion nor for the selectivity, when comparing the results from original grain size catalysts, as well as when comparing activated carbons only. All the trends we observed and described in the previous paragraphs are preserved: Rh/AC1 catalysts and AC1 carbons are those that induce the higher formation of by-products, whereas Rh/AC3 catalysts are those more selective to benzaldehyde, although with the lower conversion. And Rh/AC2 are the materials intermediate between these two. Any pre-treatment with HNO_3 lead to a higher catalytic activity and no actual trend is present from a HCl pre-treatment. In view of this, we conclude all of the results reported so far as validated, and grain size effects are not operating or negligible for our catalysts under our reaction conditions.

3. Conclusions

In the current work we have demonstrated that Rh can have the potential to be used for the oxidation of benzyl alcohol to benzaldehyde. By using a straightforward impregnation protocol, and activated carbons as supports, strong metal support interactions were able to affect the final particle size and distribution of Rh nanoparticles, with effect on the final activity of these materials. In particular, pre-treatments of the activated carbon supports with HNO_3 were capable to reduce the Rh particle size or to lead to a narrower particle size distribution, whereas treatments with HCl either had no effect or sintered the metal nanoparticles. In turn it was also possible to increase the activity of Rh/AC based materials by pre-treatment with HNO_3 while still preserving good selectivity towards benzaldehyde, with the smaller the particle size, the higher the activity. We ascribe these effects to changes in particle size to an increase or a site blocking of nanoparticle nucleation centres respectively, with probably carboxylic acids as the most likely nucleation centre for Rh species. By using these pre-treatments we also identified an upper limit for the size of Rh nanoparticles to be active for the oxidation for benzyl alcohol to benzaldehyde in the range of ca. 30 nm. We believe these data to be useful information for the development of oxidation catalysts based on this metal, and contribute to add Rh in the toolkit of metals capable to carry out oxidation reactions. In fact although our catalysts are not optimised yet, and this study represent a proof of concept on how to transform a reducing catalyst to an oxidizing species, we should nevertheless consider that our catalytic tests did not make use of any base [82], nor pressurised O_2 systems [83], nor at present, more sophisticated preparation methods like sol immobilization [84, 85] which if applied to Rh should be able to lead to a narrower and more uniform product distribution. Given these premises we consider our catalyst to be competitive with more known Au, Pd or Pt based catalysts for this reaction [86-88]. Furthermore, this study may pave the way for the exploitation of this metal for alcohol oxidation with implications beyond the current study.

Disclosure statement

The authors declare no competing financial interests.

Acknowledgements

The authors thank Prof. Iain Coldham (University of Sheffield) for careful reading of the manuscript and useful suggestions. Mr. Simon Thorpe and Mr. Neil Bramall for help and support at the Mass Spectrometry Service and elemental analysis of the University of Sheffield. TEM images were acquired at the University of Bradford, with TEM part of an institutional EPSRC Capital Grant EP/L027011/1, for which P.D.C. is the principal investigator. XPS data were acquired at the National EPSRC XPS Users' Service (NEXUS), an EPSRC Mid-Range Facility. The National Institute of Advanced Industrial Science and Technology (AIST), Japan is acknowledged for the Spectral Database for Organic Compounds, for ^{1}H NMR and MS. This work is supported financially by the University of Sheffield (grants CHM-313485 and CHM-316178) and the Royal Society (grant 148429).

References

[1] S. Cao, F. Tao, Y. Tang, Y. Li, J. Yu, Chem. Soc. Rev. 45 (2016) 4747–4765.

[2] S.C. Bourque, F. Maltais, W.-J. Xiao, O. Tardif, H. Alper, P. Arya, L.E. Manzer, J. Am. Chem. Soc. 121 (1999) 3035–3038.

[3] R.J. Farrauto, R.M. Heck, Catal. Today 51 (1999) 351–360.

[4] S. Zhang, C. Guo, Q. Qian, G. Yuan, Catal. Commun. 9 (2008) 853–858.

[5] J.O. Weston, H. Miyamura, T. Yasukawa, D. Sutarma, C.A. Baker, P.K. Singh, M. Bravo-Sanchez, N. Sano, P.J. Cumpson, Y. Ryabenkova, S. Kobayashi, M. Conte, Catal. Sci. Technol. 7 (2017) 3985–3998.

[6] T. Mallat, A. Baiker, Annu. Rev. Chem. Biomol. Eng. 3 (2012) 11–28.

[7] T. Mallat, A. Baiker, Chem. Rev. 104 (2004), 3037–3058.

[8] F. Pinna, Catal. Today 41 (1998) 129–137.

[9] Z. Hou, N. Theyssen, W. Leitner, Green Chem. 9 (2007) 127–132.

[10] I.E. Beck, V.I. Bukhtiyarov, I.Y. Pakharukov, V.I. Zaikovsky, V.V. Kriventsov, V.N. Parmon, J. Catal., 268 (2009) 60–67.

[11] M. Conte, A.F. Carley, C. Heirene, D.J. Willock, P. Johnston, A.A. Herzing, C.J. Kiely, G.J. Hutchings, J. Catal. 250 (2007) 231–239.

[12] K. Köhler, R.G. Heidenreich, J.G.E. Krauter, J. Pietsch, Chem. Eur. J. 8 (2002) 622–631.

[13] M. Conte, J.A. Lopez-Sanchez, Q. He, D.J. Morgan, Y. Ryabenkova, J.K. Bartley, A.F. Carley, S.H. Taylor, C.J. Kiely, K. Khalid, G.J. Hutchings, Catal. Sci. Technol. 2 (2012) 105–112.

[14] M. Conte, A.F. Carley, G. J. Hutchings, Catal. Lett. 124 (2008) 165–167.

[15] M. Conte, C.J. Davies, D.J. Morgan, T.E. Davies, D.J. Elias, A.F. Carley, P. Johnston, G.J. Hutchings, J. Catal. 297 (2013) 128–136.

[16] J.S. Noh, J.A. Schwarz, Carbon 28, (1990) 675–682.

[17] A. Obuchi, A. Ohi, M. Nakamura, A. Ogata, K. Mizuno, H. Ohuchi, Appl. Catal. B: Environ. 2 (1993) 71–80.

[18] Y. Nagao, Y. Nakahara, T. Sato, H. Iwakura, S. Takeshita, S. Minami, H. Yoshida, M. Machida, ACS Catal. 5 (2015) 1986–1994.

[19] R.A. Sheldon, I.W.C.E. Arends, A. Dijksman, Catal. Today 57 (2000) 157–166.

[20] L. Prati, P. Spontoni, A. Gaiassi, Top. Catal. 52 (2009) 288–296.

[21] N. Dimitratos, J.A. Lopez-Sanchez, D. Morgan, A.F. Carley, R. Tiruvalam, C.J. Kiely, D. Bethell, G.J. Hutchings, Phys. Chem. Chem. Phys. 11 (2009) 5142–5153.

[22] J.M. Hoover, B.L. Ryland, S.S. Stahl, J. Am. Chem. Soc. 135 (2013) 2357–2367.

[23] B. Wang, M. Lin, T.P. Ang, J. Chang, Y. Yang, A. Borgna, Catal. Commun. 25 (2012) 96–101.

[24] M. Conte, A.F. Carley, G. Attard, A.A. Herzing, C.J. Kiely, G.J. Hutchings, J. Catal. 257 (2008) 190–198.

[25] G.D. Robertson Jr., D.M. Mason, W.H. Corcoran, J. Phys. Chem. 59 (1955) 683–690.

[26] M. Conte, C.J. Davies, D.J. Morgan, T.E. Davies, A.F. Carley, P. Johnston, G.J. Hutchings, Catal. Sci. Technol. 3 (2013) 128–134.

[27] O.A. Ekpete, M. Horsfall Jr., Res. J. Chem. Sci. 1 (2011) 10–17.

[28] H.E. Gottlieb, V. Kotlyar, A. Nudelman, J. Org. Chem. 62 (1997) 7512–7515.

[29] M.J. Frisch, G.W. Trucks, H.B. Schlegel, G.E. Scuseria, M.A. Robb, J.R. Cheeseman, G. Scalmani, V. Barone, B. Mennucci, G.A. Petersson, H. Nakatsuji, M. Caricato, X. Li, H.P. Hratchian, A.F. Izmaylov, J. Bloino, G. Zheng, J.L. Sonnenberg, M. Hada, M. Ehara, K. Toyota, R. Fukuda, J. Hasegawa, M. Ishida, T. Nakajima, Y. Honda, O. Kitao, H. Nakai, T. Vreven, J.A. Montgomery Jr., J.E. Peralta, F. Ogliaro, M.J. Bearpark, J. Heyd, E.N. Brothers, K.N. Kudin, V.N. Staroverov, R. Kobayashi, J. Normand, K. Raghavachari A.P., Rendell, J.C. Burant, S.S. Iyengar, J. Tomasi, M. Cossi, N. Rega, N.J. Millam, M. Klene, J.E. Knox, J.B. Cross, V. Bakken, C. Adamo, J. Jaramillo, R. Gomperts, R.E. Stratmann, O. Yazyev, A.J. Austin, R. Cammi, C. Pomelli, J.W. Ochterski, R.L. Martin, K. Morokuma, V.G. Zakrzewski, G.A. Voth, P. Salvador, J.J. Dannenberg, S. Dapprich, A.D. Daniels, O. Farkas, J.B. Foresman, J.V. Ortiz, J. Cioslowski, D.J. Fox, Gaussian 09, Revision D.01; Gaussian, Inc.: Wallingford, CT, 2009.

[30] M.M. Conradie, J. Conradie, Inorg. Chim. Acta, 362 (2009) 519–530.

[31] J. Narbutt, W.P. Oziminski, Dalton Trans. 41 (2012) 14416–14424.

[32] P. Stephens, F. Devlin, C. Chabalowski, M.J. Frisch, J. Phys. Chem. 98 (1993) 11623–11627

[33] T. Ahrens, M. Ahrens, T. Braun, B. Braun, R. Herrmann, Dalton Trans. 45 (2016), 4716–4728.

[34] D.N. Briggs, K.H. Lawrence, A.T. Bell, Appl. Catal. A: Gen. 366 (2009) 71–83.

[35] C. Sepúlveda, R. García, P. Reyes, I.T. Ghampson, J.L.G. Fierro, D. Laurenti, M. Vrinat, N. Escalona, Appl. Catal. A: Gen. 475 (2014) 427–437.

[36] M. Horgnies, I. Dubois-Brugger, N.J. Krou, I. Batonneau-Gener, T. Belin, S. Mignard, Eur. Phys. J. Spec. Top. 224 (2015) 1985–1994.

[37] S.L. Barbosa, M. Ottone, M.C. Santos, G.C. Junior, C.D. Lima, G.C. Glososki, N.P. Lopes, S.I. Klein, Catal. Commun. 68 (2015) 97–100.

[38] N. Candu, M. Florea, S.M. Coman, V.I. Parvulescu, Appl. Catal. A: Gen. 393 (2011) 206–214.

[39] M. Conte, H. Miyamura, S. Kobayashi, V. Chechik, Chem. Commun. 46 (2010) 145–147.

[40] J.-P. Morel, N. Marmier, C. Hurel, N. Morel-Desrosiers J. Colloid Interf. Sci. 298 (2006) 773–779.

[41] E. Cao, M. Sankar, E. Nowicka, Q. He, M. Morad, P.J. Miedziak, S.H. Taylor, D.W. Knight, D. Bethell, C.J. Kiely, A. Gavriilidis, G. J. Hutchings, Catal. Today, 203 (2013) 146–152.

[42] C. Della Pina, E. Falletta, Michele Rossi, J. Catal. 260 (2008) 384–386.

[43] R. T. Kumar, N. C. S. Selvam, C. Ragupathi, L. J. Kennedy, J. J. Vijaya, Powder Technol. 224 (2012) 147–154.

[44] C. Ragupathi, J. J, Vijaya, R. T. Kumar, L. J. Kennedy, J. Mol. Struct. Volume 1079 (2015) 182–188.

[45] M. Martin-Martinez, M.F.F. Barreiro, A.M.T. Silva, J.L. Figueiredo, J.L. Faria, H.T. Gomes, Appl. Catal. B: Environ. 219 (2017) 372–378.

[46] H.T. Gomes, S.M. Miranda, M.J. Sampaio, J.L. Figueiredo, A.M.T. Silva, J.L. Faria, Appl. Catal. B: Environ. 106 (2011) 390–397.

[47] C. Gabaldón, P. Marzal, J. Ferrer, A. Seco, Wat. Res. 30 (1996) 3050–3060.

[48] F. Rodríguez-Reinoso, Carbon 36 (1998) 159–175.

[49] T. Gong, L. Qin, W. Zhang, H. Wan, J. Lu, H. Feng, J. Phys. Chem. C, 119 (2015) 11544−11556.

[50] S.R. Joshi, K. L. Kataria, S. B. Sawant, J. B. Joshi, Ind. Eng. Chem. Res. 44 (2005) 325–333.

[51] J. P. Chen and S. Wu, Langmuir 20 (2004) 2233–2242.

[52] A. Borgna, F. Le Normand, T.F. Garetto, C.R. Apesteguía, B. Moraweck, Stud. Surf. Sci. Catal. 126 (1999) 179–186.

[53] K. An, G.A. Somorjai, ChemCatChem 4 (2012) 1512–1524.

[54] K. Wilson, H. Yang, C.W. Seo and W.E. Marshall, Bioresour. Technol. 97 (2006) 2266–2270.

[55] R.L. Vaughan Jr., J. Yang, L.E. Le Mire, B.E. Reed, Adsorpt. Sci. Technol. 25 (2007) 295–310.

[56] B. Kordić, B. Jović, J. Tričković, M. Kovačević, J. Mol. Liq. 259 (2018) 7–15.

[57] H. Masuda, K. Gotoh, Adv. Powder Technol. 10 (1999) 159–173.

[58] C. Yu, S. Koh, J.E. Leisch, M.F. Toney, P. Strasser, Faraday Discuss. 140 (2009) 283–296.

[59] Z. Jian-Min, M. Fei, X. Ke-Wei, Chinese Phys. 13 (2004) 1082–1090.

[60] R. Fisker, J.M. Carstensen, M.F. Hansen, F. Bødker, S. Mørup, J. Nanopart. Res. 2 (2000) 267–277.

[61] L.B. Kiss, J. Söderlund, G.A. Niklasson, C.G. Granqvist, Nanotechnology, 10 (1999) 25–28.

[62] M. Barberio, P. Antici, Sci. Rep. 7 (2017) 41372.

[63] A.M. Maley, G.J. Lu, M.G. Shapiro, R.M. Corn, ACS Nano 11 (2017) 7447–7456.

[64] J. Li, L. Ma, X. Li, C. Lu, H. Liu, Ind. Eng. Chem. Res. 44 (2005) 5478–5482.

[65] D. Lennon, D.T. Lundie, S.D. Jackson, G.J. Kelly, S.F. Parker, Langmuir 18 (2002) 4667–4673.

[66] A.M. Puziy, O.I. Poddubnaya, R.P. Socha, J. Gurgul, M. Wisniewski, Carbon 46 (2008) 2113–2123.

[67] O. Senneca, P. Russo, P. Salatino, S. Masi, Carbon 35 (1997) 141–151.

[68] M.L. Miller R.W. Linton, Anal. Chem. 57 (1985) 2314–2319.

[69] A.P. Dementjev, A. de Graaf, M.C.M. van de Sanden, K.I. Maslakov, A.V. Naumkin, A.A. Serov, Diamond Relat. Mater. 9 (2000) 1904–1907.

[70] S. Akhter, K. Allan, D. Buchanan, J.A. Cook, A. Campion, J.M. White, Appl. Surf. Sci., 36 (1988-89) 241–258.

[71] E. Desimoni, B. Brunetti, Chemosensors 3 (2015) 70–117.

[72] H.S. Swanson, R.K. Fuyat, G.M. Ugrinic, US Natl. Bur. Stand. Circ. (1953), in: International Centre for Diffraction Data, Powder Diffraction File, Entry 5-685, 1996.

[73] K. Neininger,W. Eysel, Grant-in-Aid Heidelberg, (1990) in: International Centre for Diffraction Data, Powder Diffraction File, Entry 41-541, 1996.

[74] J. Liu, Z. Zhao, J. Wang, C. Xu, A. Duan, G. Jiang, Q. Yang, Appl. Catal. B: Environ. 84 (2008) 185–195.

[75] R.T. Kumar, P. Suresh, N.C.S. Selvam, L.J. Kennedy, J.J. Vijaya, J. Alloy. Compd. 522 (2012) 39–45

[76] H.S. Swanson, R.K. Fuyat, G. M. Ugrinic, US Natl. Bur. Stand. Circ. (1954) in: International Centre for Diffraction Data, Powder Diffraction File, Entry 5-490, 1996.

[76] F. Rodriguez-Reinoso, Carbon. 36 (1998) 159–175.

[77] H.S. Swanson, R.K. Fuyat, G. M. Ugrinic, US Natl. Bur. Stand. Circ. (1954) in: International Centre for Diffraction Data, Powder Diffraction File, Entry 5-490, 1996.

[78] A. Dankekar, R.T.K. Baker, M.A. Vannice, Carbon 36 (1998) 1821–1831.

[79] A.S. Aricó. V. Antonucci, M. Minutoli, N. Giordano, Carbon 27 (1989) 337–347.

[80] L.M. Cohen, M.R. Denison, N. Gat, A.B. White, Combust. Sci. Technol. 27 (1981) 79–82.

[81] M. Mandić, B. Todić, L. Živanić, N. Nikačević, D. B. Bukur, Ind. Eng. Chem. Res. 56 (2017) 2733−2745.

[82] M. Besson, P. Gallezot, Catal. Today, 57 (2000) 127−141.

[83] C. Keresszegi, D. Ferri, T. Mallat, A. Baiker, J. Phys. Chem. B 109 (2005) 958−967.

[84] N. Dimitratos, J.A.Lopez-Sanchez, D. Morgan, A.F. Carley, R. Tiruvalam, C.J. Kiely, D. Bethell, G.J. Hutchings, Phys. Chem. Chem. Phys. 11 (2009) 5142–5153.

[85] C. Della Pina, E. Falletta, M. Rossi, J. Catal. 260 (2008) 384–386.

[86] J. Muzart, Tetrahedron, 59 (2003) 5789–5816.

[87] C. Parmeggiani, F. Cardona, Green Chem. 14 (2012) 547–564.

[88] P. Haider, B. Kimmerle, F. Krumeich, W. Kleist, J.-D. Grunwaldt, A. Baiker, Catal. Lett. 125 (2008) 169–176.

Appendix A. Supplementary Data file available: ^{1}H-NMR spectra, GC/MS chromatograms and fragmentation patterns, XPS spectra, particle size distributions. Details of product characterization, and analysis of the reaction mixtures. Figs. S1 to S19, Tables S1 to S14 and equations S1 to S13.

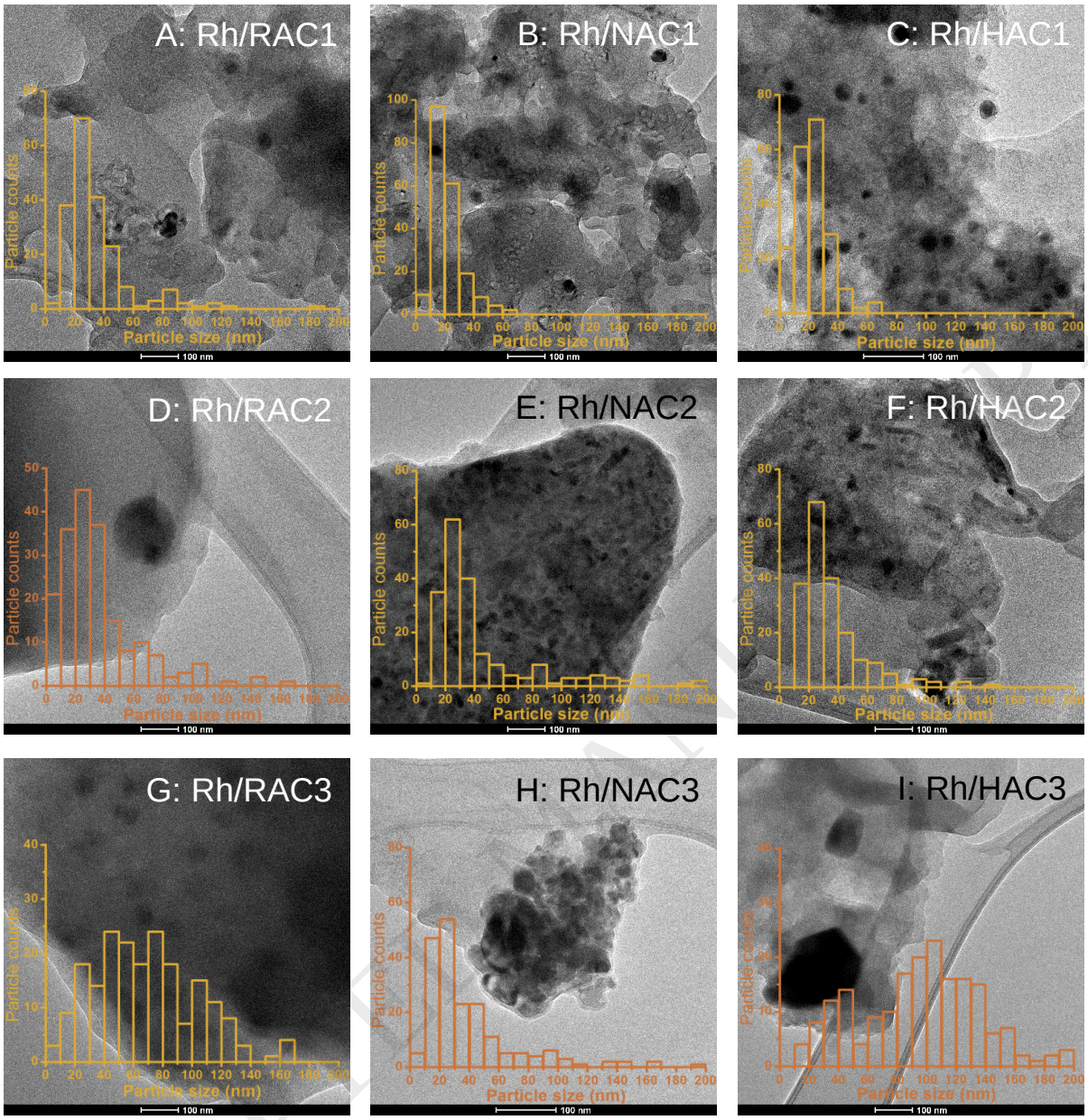

Fig. 1. Representative transmission electron microscopy images and particle size distribution histograms of Rh nanoparticles for: (A) Rh/RAC1 catalyst, average particles size (log-normal) d = 30 nm, (B) Rh/NAC1 catalyst, average particles size (Gaussian) d = 23 nm, (C) Rh/HAC1 catalyst, average particles size (log-normal) d = 20 nm; (D) Rh/RAC2 catalyst, average particles size (log-normal) d = 29 nm, (E) Rh/NAC2 catalyst, average particles size (log normal) d = 31 nm, (F) Rh/HAC2 catalyst, average particles size (log-normal) d = 36 nm; (G) Rh/RAC3 catalyst, average particles size (Gaussian) d = 69 nm, (H) Rh/NAC3 catalyst, average particles size (log-normal) d = 32 nm, (I) Rh/HAC3 catalyst, average particles size (Gaussian) d = 106 nm.

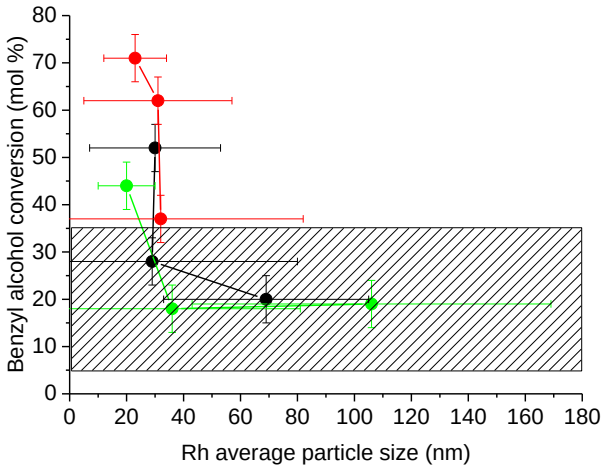

Fig. 2. Overall conversion for all Rh/C catalysts versus average Rh particle size (best fitting values between Gaussian and log-normal distribution are inserted). (●) Catalysts prepared on untreated activated carbons, (●) catalysts prepared on carbons pre-treated with HNO_3, and (●) catalysts prepared on carbons pre-treated with HCl. Dashed area: overall activity from all the carbons supports including treated and untreated samples.

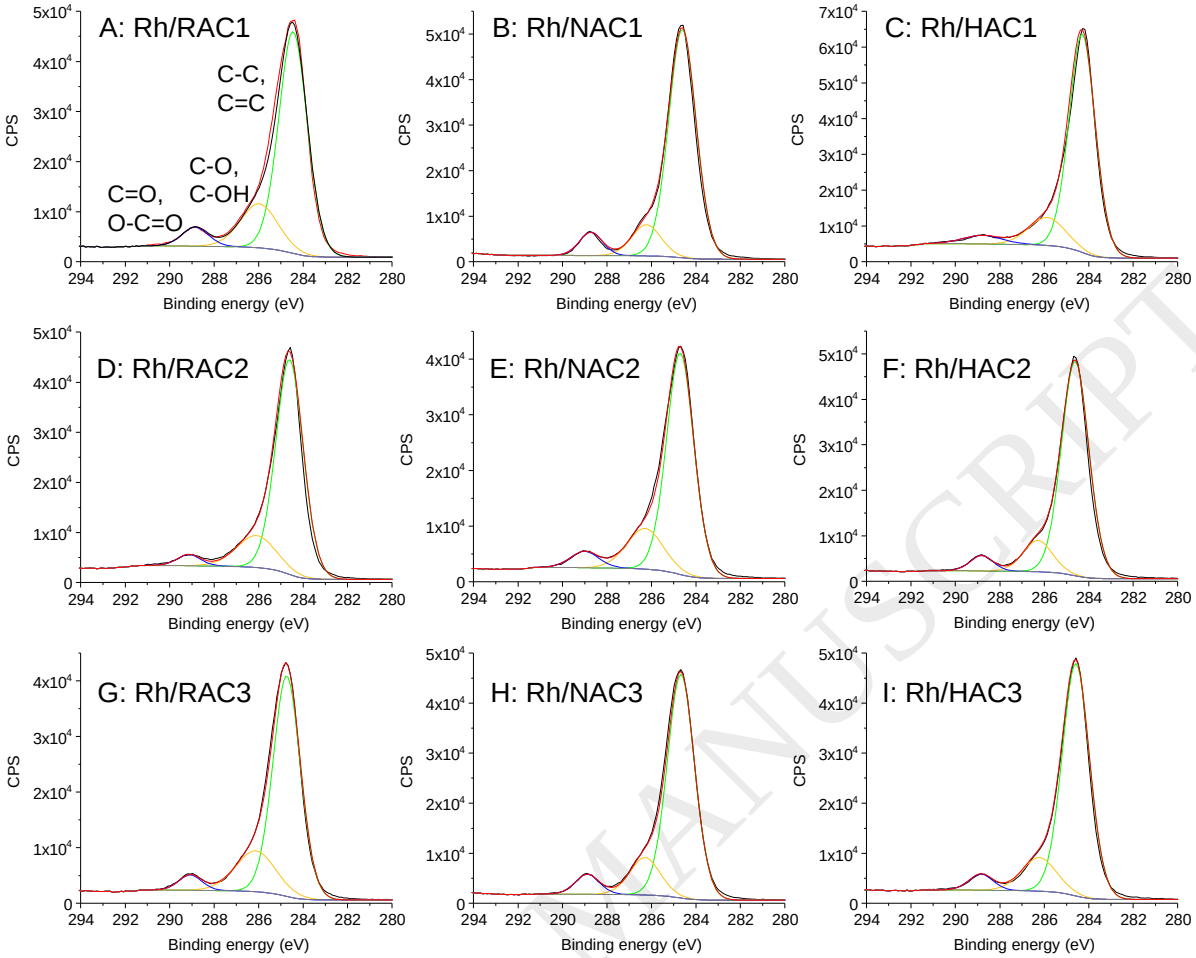

Fig. 3. XPS spectra, simulation and peak fitting of the C1s region for : (A) Rh/RAC1, (B) Rh/NAC1, (C) Rh/HAC1, (D) Rh/RAC2, (E) Rh/NAC2, (F) Rh/HAC2, (G) Rh/RAC3 and (H) Rh/NAC3. C1s signal peak fitted considering three groups of chemical species: (i) C-C and C=C bonds (284.6 ± 0.2 eV), (ii) C-OH and C-O groups (286 ± 0.2 eV), and (iii) C=O and O-C=O groups (288.2 ± 0.2) exemplified in figure S17A for Rh/RAC1.

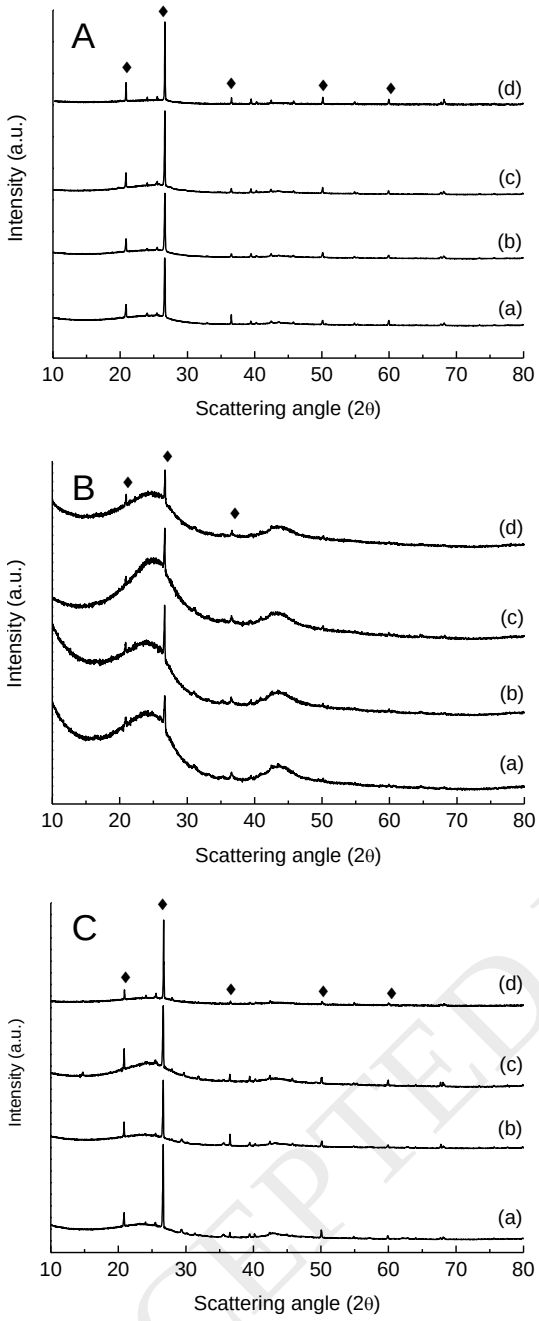

Fig. 4. XRPD patterns for: (A) Rh/AC1 catalysts and fresh AC1 for comparison: (a) untreated AC1, (b) Rh/RAC1, (c) Rh/NAC1, (d) Rh/HAC1; (B) Rh/AC2 catalysts and fresh AC2 for comparison: (a) untreated AC2, (b) Rh/RAC2, (c) Rh/NAC2, (d) Rh/HAC2; (C) Rh/AC3 catalysts and fresh AC3 for comparison: (a) untreated AC3, (b) Rh/RAC3, (c) Rh/NAC3, (d) Rh/HAC3. No Rh or Rh_2O_3 are detected in these XRD patterns. Facets typical of SiO_2 (♦) quartz, were detected.

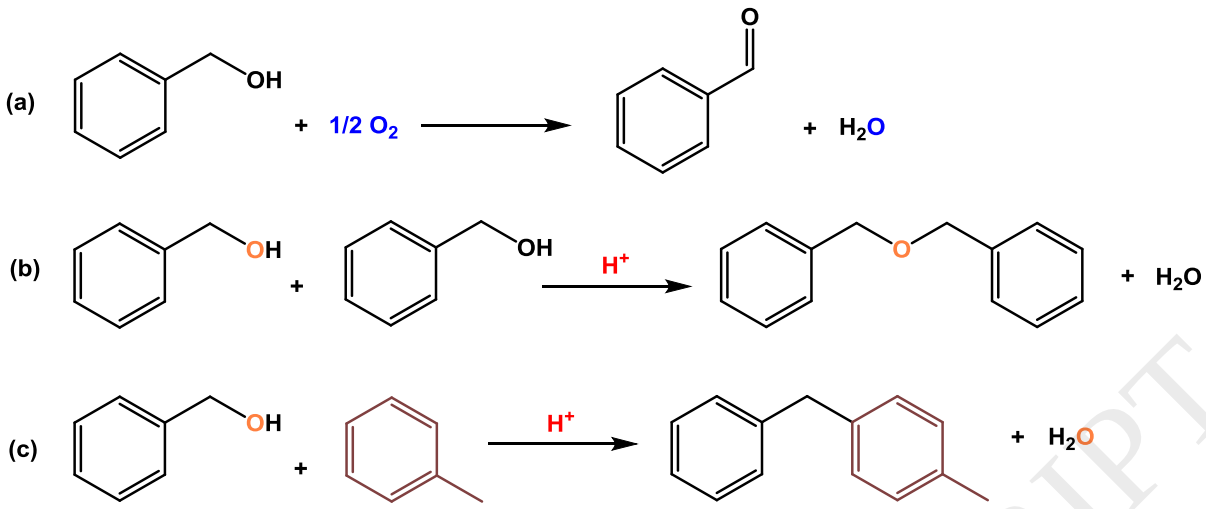

Scheme 1. Possible parallel reactions in the oxidation of benzyl alcohol to benzaldehyde for our Rh/ACs catalysts and if in the presence of Brønsted acid centres: (a) oxidation of benzyl alcohol to benzaldehyde (no acid centre required) a water formation as by-product; (b) condensation of two molecules of benzyl alcohol to form one molecule of dibenzyl ether, and elimination of a water molecule; (c) benzylation reaction involving the addition of a benzylic carbocation (not shown) from benzyl alcohol to a toluene molecule, and elimination of a water molecule to form methyl-diphenylmethane isomers (in this scheme the isomer 4- is reported).

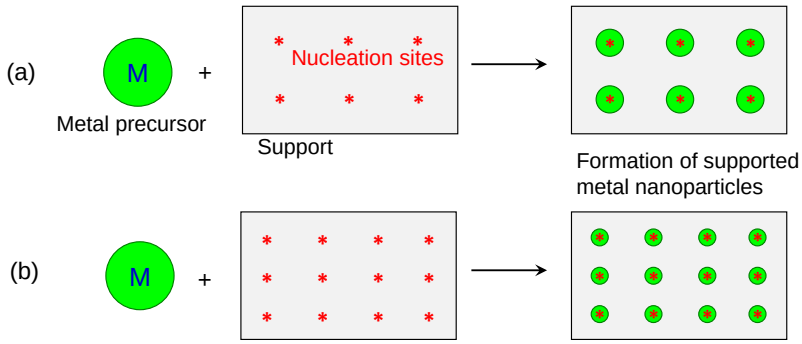

Scheme 2. Effect of the increase of nucleation centres on particle size. (a) Deposition and nucleation of the metal precursor on a support with a generic number of nucleation sites, (b) if the same initial amount of metal precursor can distribute on a higher number of nucleation sites, and if these are evenly distributed, smaller particles, on average, will be obtained.

Table 1. Catalytic tests for the oxidation of benzyl alcohol in toluene by Rh/RAC catalysts and untreated activated carbons in the absence of Rh (RAC1 = Darco-12, RAC2 = Norit GAC 1240, and RAC3 = Norit SA2). Reaction conditions: T = 100 °C, P = atmospheric pressure of air, reaction time t = 24 h, molar metal-to-substrate M:S = 1:100. Carbon mass balance > 95%. MDM = methyl-diphenylmethane isomers. All selectivity values are normalised to 100% from ^{1}H NMR data. Blank: test in the absence of any catalyst and use of reaction mixture only.

Catalyst	**Conversion (%)**	**Selectivity (%)**		
		Benzaldehyde	Dibenzyl ether	MDM
Rh/RAC1	52	58	32	10
Rh/RAC2	28	95	5	0
Rh/RAC3	20	100	0	0
RAC1	15	62	29	9
RAC2	9	99	1	0
RAC3	7	100	0	0
$RhCl_3 \cdot xH_2O$	3	100	0	0
Blank	5	100	0	0

Table 2. Catalytic tests for the oxidation of benzyl alcohol in toluene by Rh/NACcatalysts, where NAC stands for activated carbons pre-treated with HNO_3 before Rh impregnation. (NAC1 = Darco-12, NAC2 = Norit GAC 1240, and NAC3 = Norit SA2). Reaction conditions: T = 100 ºC, P = atmospheric pressure of air, reaction time t = 24 h, activated carbon mass same as for Rh/C catalysts. Carbon mass balance > 95%, MDM = methyl-diphenylmethane isomers. All selectivity values are normalised to 100% from ^{1}H NMR data.

Catalyst	**Conversion (%)**	**Selectivity (%)**		
		Benzaldehyde	Dibenzyl ether	MDM
Rh/NAC1	71	50	31	19
Rh/NAC2	62	60	32	9
Rh/NAC3	37	100	0	0
NAC1	33	27	55	18
NAC2	35	33	48	19
NAC3	15	100	0	0

Table 3. Catalytic tests for the oxidation of benzyl alcohol in toluene by Rh/HAC catalysts, where HAC stands for activated carbons pre-treated with HCl before Rh impregnation. (HAC1 = Darco-12, HAC2 = Norit GAC 1240, and HAC3 = Norit SA2). Reaction conditions: T = 100 ^{o}C, P = atmospheric pressure of air, reaction time t = 24 h, activated carbon mass same as for Rh/C catalysts. Carbon mass balance > 95%, MDM = methyl-diphenylmethane isomers. All selectivity values are normalised to 100% from ^{1}H NMR data.

Catalyst	**Conversion (%)**	**Selectivity (%)**		
		Benzaldehyde	Dibenzyl ether	MDM
Rh/HAC1	44	66	27	6
Rh/HAC2	18	59	41	0
Rh/HAC3	19	100	0	0
HAC1	21	92	4	4
HAC2	5	94	6	0
HAC3	3	100	0	0

Table 4. Rh average particle size from TEM analysis of all Rh/AC catalysts. Comparison of particle size by using a Gaussian distribution model and a log-normal distribution model (see Appendix A, Supplementary Data File, Figs. S17 and S18). Particle size values in bold represent the best fitting.

Catalyst	**Rh average particle size (nm) Gaussian distribution**	**Rh average particle size (nm) Log-normal distribution**
Rh/RAC1	35	**30**
Rh/RAC2	43	**29**
Rh/RAC3	**69**	58
Rh/NAC1	**23**	20
Rh/NAC2	36	**31**
Rh/NAC3	46	**32**
Rh/HAC1	22	**20**
Rh/HAC2	48	**36**
Rh/HAC3	**106**	90

Table 5. XPS analysis of composition ratio for all the Rh/AC catalysts, by deconvolution of XPS C1s signals into three components: single and double C-C bonds, alcohol and ethers, carbonyl, esters and acids.

Catalyst	**Composition ratio**		
	C-C and C=C	C-OH and C-O	C=O and O-C=O
Rh/RAC1	78.4	15.5	6.1
Rh/NAC1	80.6	12.4	7.0
Rh/HAC1	79.1	15.9	5.0
Rh/RAC2	80.0	16.2	3.7
Rh/NAC2	76.9	17.0	6.0
Rh/HAC2	80.9	14.1	5.0
Rh/RAC3	78.0	17.8	4.2
Rh/NAC3	80.0	14.7	6.3
Rh/HAC3	78.4	15.5	6.1